Eur. Phys. J. Appl. Phys. **43**, 357–361 (2008)
DOI: 10.1051/epjap:2008100

THE EUROPEAN PHYSICAL JOURNAL APPLIED PHYSICS

Influence of interfacial oxygen on single-crystal magnetic tunnel junctions

F. Bonell[a], A.M. Bataille, S. Andrieu, C. Tiusan, B. Kierren, G. Lengaigne, and D. Lacour

Laboratoire de Physique des Matériaux, BP 239, 54506 Vandoeuvre-lès-Nancy, France

Received: 15 January 2008 / Accepted: 21 April 2008
Published online: 19 June 2008)

Abstract. The influence of adsorbed oxygen at the first interface of single-crystal Fe(001)/MgO(001)/Fe(001) magnetic tunnel junctions is investigated. Firstly, the adsorption kinetics of O_2 on the Fe(001) surface is studied in the monolayer regime by X-ray photoelectrons spectroscopy and scanning tunnelling microscopy experiments. We show that different species exist at the oxidized surface. The tunnel magneto-resistance of oxygen-doped magnetic tunnel junctions is found to decrease but remains large even for oxygen coverages exceeding one monolayer.

PACS. 85.75.-d Magnetoelectronics; spintronics: devices exploiting spin polarized transport or integrated magnetic fields – 68.37.Ef Scanning tunneling microscopy – 68.43.-h Chemisorption/physisorption: adsorbates on surfaces

1 Introduction

During the last five years, the large tunnel magneto-resistance (TMR) measured at room temperature in Fe(001)/MgO(001)/Fe(001) single-crystal magnetic tunnel junctions (MTJs) opened new interesting perspectives for the MTJ integration in data storage devices and sensors. In these single crystal systems, as theoretically predicted [1], the large TMR effect is related to the symmetry dependent electronic transport. The propagating electrons are selected, in terms of the symmetry of their Bloch wave functions, within the bcc Fe electrodes. The single crystal MgO tunnel barrier provides a symmetry dependent attenuation rate for the wave functions matched at the Fe/MgO interfaces. Then, in the asymptotic regime, corresponding to a thick MgO insulating barrier (typically 2.5 nm), one can roughly consider that the only tunnelling electrons propagate perpendicularly to interfaces along the [001] direction of the crystal (electrons with $k_{//} = 0$). This corresponds to the Δ direction of the reciprocal lattice. Then, the large TMR arises from the fact that the bcc Fe is a half-metal with respect to the Δ_1 symmetry Bloch state, which has the smallest decay-rate within the MgO barrier compared to other existing electronic symmetries [1].

However, the discrepancy between the theoretical TMR (more than 1000%) and reported experimental values (below 200% at 300 K and 340% at 10 K) is high [2–4]. Likewise, several electronic transport features cannot be explained within a simple theoretical framework describing a perfect MTJ. Additional refinements have been introduced pointing out the imperfect filtering of the barrier and more recently, the crucial influence on the tunnelling of the interfaces. The modulation of the interfacial electronic and chemical structure represents a powerful tool to modulate the spin polarized transport properties in single crystal MTJs.

Firstly, as predicted by the theory [5], the contribution to the tunnelling of the Fe interfacial minority-spin density of state has been experimentally demonstrated [6]. Secondly, specific studies have been focused on the chemical contamination of interfaces. Carbon and oxygen may therefore contaminate the Fe/MgO interface in a Fe/MgO/Fe MTJ [7–9]. The oxygen which comes from a residual pressure in the growth chamber or from the initial stages of MgO deposition [9] may have a drastic effect on the TMR amplitude, as theoretically predicted [10].

However, one can also take advantage of the interfacial impurities to skilfully tune the electronic structure of the Fe(001)/MgO(001)/Fe(001) MTJs. Thus, specific properties may be enhanced in order to improve the MTJ performances, to develop new characteristics or, from a fundamental point of view, to improve our understanding on the tunnelling mechanisms. For instance, despite a slightly reduced TMR ratio, carbon enriched MTJs present interesting TMR sign inversions with bias voltage [3] due to enhanced resonant tunnelling via the interfacial state. These C doped Fe/MgO MTJs also show important characteristics for potential device integration such as a higher output voltage [8], an extremely small 1/f noise and a large stability in electric fields (up to 10^9 V/m) [4].

[a] e-mail: frederic.bonell@lpm.u.nancy.fr

In this paper we present the first results on MTJs having an oxygen doped Fe(001)/MgO interface with a precise control of the oxygen amount. The early stages of O_2 adsorption on an Fe(001) surface have been widely studied [11–18]. Using X-ray photoelectrons spectroscopy (XPS) we show here that the existing results can be reproduced, and more importantly, that the amount of deposited oxygen can be precisely controlled in the monolayer (ML) range. The reproducibility criterion and the precise control of the oxygen amount represent important steps to build reproducible MTJ devices dedicated to study the oxygen influence on the transport. Moreover, in addition to the 'standard' XPS analysis, we perform a direct study of the morphology of oxygen-covered Fe layers by scanning tunnelling microscopy (STM). Varying the oxygen coverage, different species are identified on the surface. Finally, the effect of interfacial oxygen on the experimental TMR of Fe/MgO/Fe(001) MTJs is discussed.

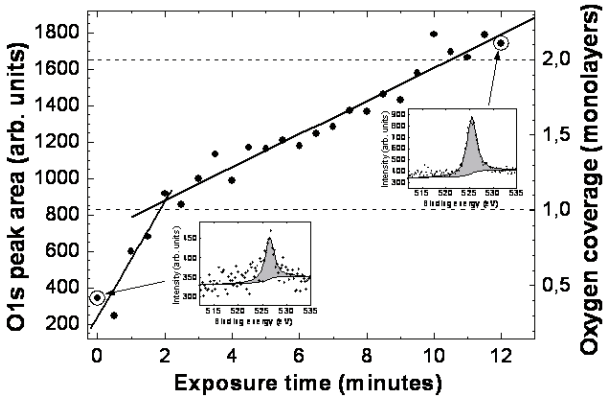

Fig. 1. Area of the O1s XPS peak versus exposition time (left axis), and corresponding oxygen coverage (right axis). Insets: experimental spectra at the beginning and the end of the adsorption process. The grey areas are reported on the left axis of the main figure.

2 Experimental

Our single-crystal multilayer stacks were prepared on MgO(001) substrates by using Molecular Beam Epitaxy (MBE) operating with a base vacuum of 8×10^{-9} Pa (6×10^{-11} Torr). After outgassing the substrate at 875 K, an MgO layer was deposited at 725 K to improve the quality of the substrate surface, and to avoid the diffusion of residual carbon through the first Fe layer [7]. The 50 nm thick bottom Fe layer was deposited at room temperature, and annealed at 725 K for 20 min, in order to obtain an atomically flat surface. Subsequently, we performed the oxygen adsorption at room temperature in a separate chamber. O_2 was introduced by a leak valve, with a partial pressure of 7×10^{-7} Pa (5×10^{-9} Torr). The amount of adsorbed oxygen was controlled during the adsorption, by monitoring the O1s peak by XPS, using a standard Al Kα source.

The STM experiments were performed in the constant current mode. They were done in a pressure of 4×10^{-8} Pa (3×10^{-10} Torr), in a chamber directly connected to the MBE chamber. We used chemically etched W tips, which were heated under UHV by Joule effect and finally shaped above the sample surface by field effect prior to oxygen adsorption.

To prevent any contamination of the bottom Fe layer during the STM analysis, the samples dedicated to the transport measurements have not been analyzed by STM. On these samples, the MgO insulating barrier was deposited just after the oxygen adsorption. For this purpose we evaporated stoichiometric MgO by electron-beam heating, at a growth rate of 0.02 nm/s. On top of the bottom smooth Fe electrode, a 2.5 nm thick MgO barrier was grown and precisely controlled using RHEED intensity oscillations. A 15 nm thick second Fe electrode was deposited on top of the MgO barrier and annealed 10 min at 475 K. The hard/soft magnetic architecture in such a MTJ, necessary to operate independently the magnetization of its electrodes, was obtained by hardening the top Fe electrode by a 20 nm thick Co over-layer. After the growth, square MTJs with sizes varying from 10×10 to 200×200 μm^2 were patterned by optical lithography and ion etching.

3 Results

3.1 XPS

Figure 1 shows a plot of the O1s peak area against exposition time. The kinetics shown here clearly exhibit the two distinct regimes reported in the literature. At very low exposures, it was shown that oxygen adsorbs into a mobile precursor state, which accounts for the high sticking probability we observed (high slope of the curve) [11–16]. The second regime is commonly explained by the growth of two-dimensional FeO islands [17,18]. We calibrated the oxygen coverage by measuring the XPS signal of the well-known P(1×1) reconstruction of oxygen on Fe(001) [13,19]. This well ordered phase was prepared by O_2 adsorption at RT and heating up to 925 K. The (1×1) surface lattice was checked with STM. This procedure was reproduced several times and gave reproducible results. We deduce from our calibration that the transition between the two regimes occurs at an oxygen coverage of 1 ± 0.1 ML (see right axis on Fig. 1). Some oxygen is always detected on "clean" iron surfaces, but we emphasize that the amount never exceeds 0.2 ML.

Concerning a possible evolution of the oxygen surface concentration, we point out that oxygen is known to be a good iron surfactant, thus no diffusion under the surface is expected. Indeed segregation to the surface when additional Fe is deposited has been reported [19]. Moreover, we checked with XPS measurements that no desorption occurs at least during one hour. Consequently, adsorbed oxygen forms a surface layer, whose coverage is well defined. Taking into account the reproducibility of the kinetics depicted in Figure 1, the uncertainty on the determination of the oxygen coverage is assumed to be ± 0.1 ML.

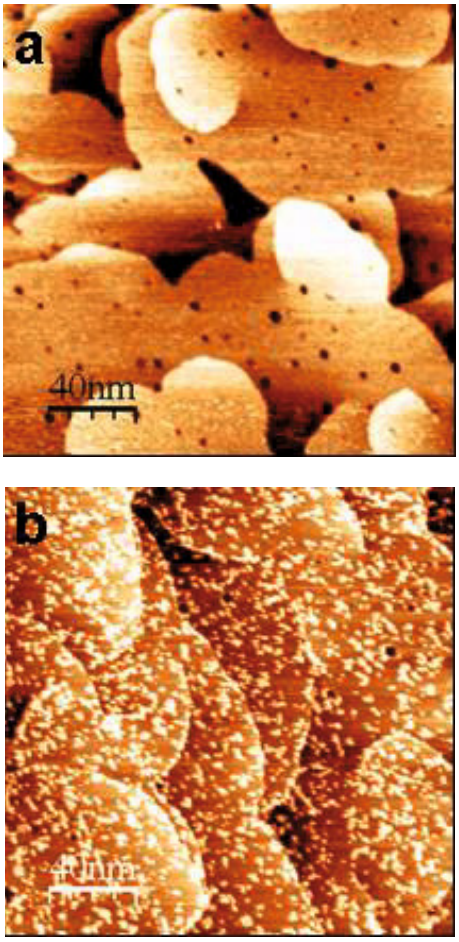

Fig. 2. (Color online) STM images of Fe(001) surfaces exposed to O_2 (tip-sample voltage: −500 mV; current: 1 nA; scale bar: 40 nm). Oxygen coverage: (a) 0.4 ± 0.1 ML, (b) 1.2 ± 0.1 ML.

3.2 STM

Figure 2 shows STM images of Fe surfaces with two different oxygen coverages. The STM image in Figure 2a (0.4 ML of oxygen) illustrates the surface morphology in the first adsorption regime. This image presents all the characteristics of a clean Fe surface. One can see large terraces bordered by monoatomic steps. These steps are curved and often link two threading dislocations. Holes can also be seen, that we ascribe to some de-wetting (since Fe growth on MgO forms 3D islands at equilibrium). The RMS roughness of such a surface is around 0.12 nm for a 200×200 nm^2 area. Actually, to improve the surface roughness and make the STM experiments easier, the Fe films shown in Figure 2 were annealed at 775 K. Slightly larger terraces and a greater density of de-wetting holes are the only differences with films annealed at 725 K. We did not detect any effect on oxygen adsorption. At very low oxygen coverages, no manifestation of adsorbed oxygen can be seen on the Fe surface. This point is in agreement with the existence of a mobile species at low concentrations.

As shown in Figure 2b (1.2 ML of oxygen), the second adsorption regime is characterized by a rather different surface morphology, since one can see numerous islands distributed on the whole surface. Let us note that the Fe atomic steps and holes remain unchanged. For such an oxygen coverage, the RMS roughness for a 200×200 nm^2 area increases up to 0.21 nm.

Other direct observations of oxidized Fe surfaces with different amounts of oxygen confirm that a gas-solid transition occurs, the critical oxygen coverage being at the monolayer. The coverage of oxide islands estimated from the STM image of Figure 2b is found to be around 30% of the whole surface. Figure 3a shows an atomically resolved image of this surface. The islands amount observed in Figure 2b is in agreement with the 1.2 ± 0.1 ML thick oxygen deposition assuming that the film is constituted of a $P(1\times1)$ oxygen phase plus 0.2 ± 0.1 ML corresponding to islands. Since these islands are well spread, and not preferentially located near steps of the Fe surface or around the de-wetting holes, the oxide formation must result from an intermixing of the oxygen adsorbates with the underlying Fe.

At this scale, in addition to the oxide islands, some mobile depletions are seen (Fig. 3b). A key point is that they always form squares or combinations of squares. Moreover, four atoms of the (1×1) lattice are seen in these depletions. These features may be explained by some additional oxygen atoms located in the hollow sites of the $P(1 \times 1)$ oxygen layer, appearing counterintuitively as depressions in the STM images. This oxygen species may be the mobile precursor also expected at coverages greater than 1 ML [11].

3.3 Magneto-transport

The magneto-transport measurements have been performed in MTJ devices patterned from the continuous stack by UV lithography and ion etching. The TMR of several Fe(001)/O/MgO(001)/Fe(001) MTJs is shown in Figure 4.

Figure 4 shows two interesting features. First, the TMR decreases with increasing the amount of interfacial oxygen. RHEED intensity oscillations clearly show a layer-by-layer growth of MgO on Fe(001) surfaces exposed to oxygen (Fig. 5). Thus, we think that the structural quality of the barrier is not involved, and that the TMR reduction is due to the electronic properties of the Fe/MgO interface. Actually, STM experiments show the presence of a $P(1 \times 1)$ oxygen overlayer which is theoretically expected to reduce the TMR by lowering the matching of electronic wave functions at the interface between the bulk Fe and MgO, and the tunnelling conductivity [10]. Another phenomenon certainly plays an important role for this oxygen induced TMR reduction. When interfacial defects are present (such as oxide islands or isolated oxygen atoms), electrons experience a local variation of the crystalline periodic potential and can be elastically scattered. The symmetry of Bloch states may be locally broken, so that the interpretations of transport measurements need to

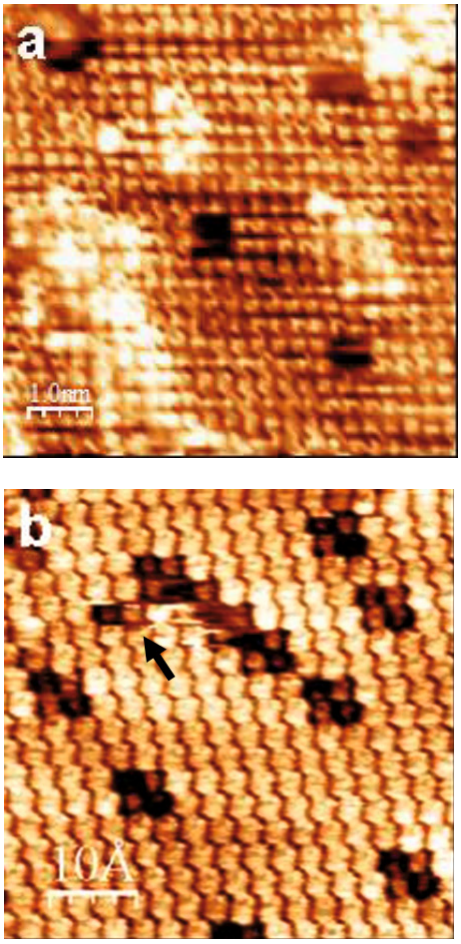

Fig. 3. (Color online) Atomic-scale STM images of the sample shown in Figure 2b. Scale bars: 1 nm. The thermal drift was not corrected. (a) tip-sample voltage: −500 mV; current: 1 nA. (b) tip-sample voltage: +42 mV; current: 1 nA. The arrow indicates an artefact due to a square depletion moving during the scan.

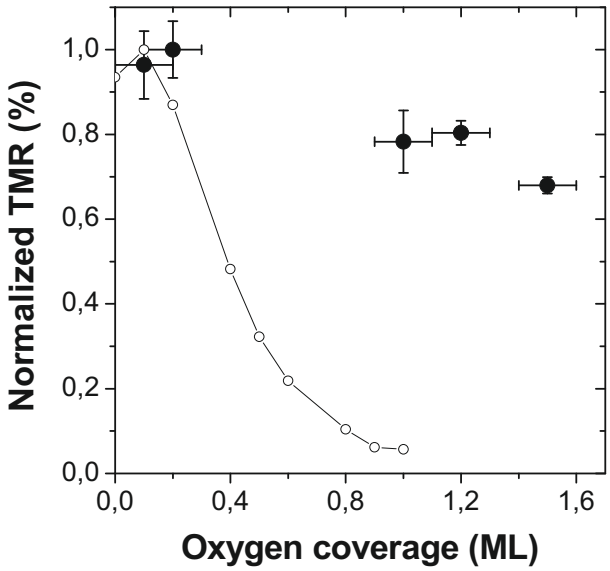

Fig. 4. Normalized tunnel magneto-resistance amplitude of Fe(001)/O/MgO(001)/Fe(001) MTJs versus oxygen coverage at the bottom Fe/MgO interface. The calculated curve is from reference 10.

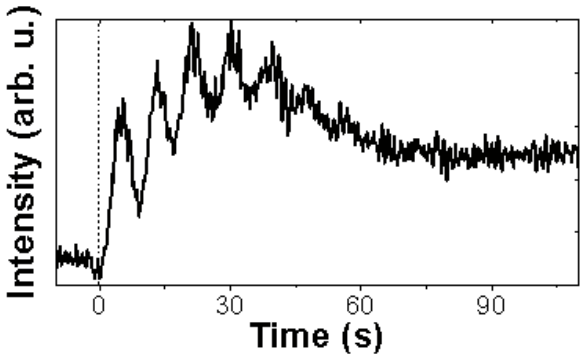

Fig. 5. RHEED intensity oscillations recorded during the growth of MgO on an Fe(001) surface with 2 ML of adsorbed oxygen.

take in consideration $k_{//}$-resolved transmission probabilities through the barrier. Therefore, the elastic scattering enhances the low tunnel conductivity in the antiparallel MTJ configuration, opening additional tunnelling channels with $k_{//} \neq 0$. This may lead to a reduction of the TMR ratio, defined as the conductivity contrast between the parallel and antiparallel MTJ states.

The second relevant result evident in Figure 4 is that the TMR remains high, even with 1.5 ML of adsorbed oxygen. This means that the effect of the interfacial oxygen is less detrimental to the TMR amplitude than expected from theoretical studies involving only ballistic transport. This may indicate that experimentally, the spin polarized transport in single crystal MTJs gets beyond the framework of the ballistic transport. Elastic and inelastic scattering events may play an important role.

4 Conclusion

The adsorption of O_2 on an Fe(001) surface and its effect on the TMR of Fe(001)/MgO(001)/Fe(001) MTJs have been studied. We show that XPS measurements during the adsorption allow us to control precisely the amount of deposited oxygen in the sub-monolayer regime. Both XPS and STM experiments show the existence of two regimes in the kinetics. Below 1 ML, oxygen is entirely in a mobile precursor state. Above 1 ML, the P(1 × 1) phase is observed. The additional oxygen atoms seem to divide up between two-dimensional oxide islands and the mobile precursor species. Concerning the consequences on magneto-transport, the TMR of MTJs with an oxygen-doped bottom Fe/MgO interface is found to decrease with the amount of oxygen. However, this reduction is not as dramatic as predicted by theoretical calculations. This consequently allows us to tune the interfacial electronic

properties of MTJs which still preserve important TMR ratios required for potential integration. Further experiments are in progress, to investigate more in details the effects of oxygen on the tunnelling mechanisms.

We would like to acknowledge F. Montaigne for his help in lithography processes.

References

1. W.H. Butler, X.-G. Zhang, T.C. Schulthess, J.M. MacLaren, Phys. Rev. B **63**, 054416 (2001)
2. C. Tiusan, F. Greullet, M. Hehn, F. Montaigne, S. Andrieu, A. Schuhl, J. Phys.: Condens. Matter **19**, 165201 (2007)
3. S. Yuasa, T. Nagahama, A. Fukushima, Y. Suzuki, K. Ando, Nat. Mater. **3**, 868 (2004)
4. R. Guerrero, D. Herranz, F.G. Aliev, F. Greullet, C. Tiusan, M. Hehn, F. Montaigne, Appl. Phys. Lett. **91**, 132504 (2007)
5. O. Wunnicke, N. Papanikolaou, R. Zeller, P.H. Dederichs, V. Drchal, J. Kudrnovský, Phys. Rev. B **65**, 064425 (2002)
6. C. Tiusan, J. Faure-Vincent, C. Bellouard, M. Hehn, E. Jouguelet, A. Schuhl, Phys. Rev. Lett. **93**, 106602 (2004)
7. M. Sicot, S. Andrieu, C. Tiusan, F. Montaigne, F. Bertran, J. Appl. Phys. **99**, 08D301 (2006)
8. C. Tiusan, M. Sicot, M. Hehn, C. Belouard, S. Andrieu, F. Montaigne, A. Schuhl, Appl. Phys. Lett. **88**, 62512 (2006)
9. H.L. Meyerheim, R. Popescu, J. Kirschner, N. Jedrecy, M. Sauvage-Simkin, B. Heinrich, R. Pinchaux, Phys. Rev. Lett. **87**, 076102 (2001)
10. X.G. Zhang, W.H. Butler, A. Bandyopadhyay, Phys. Rev. B **68**, 092402 (2003)
11. G.W. Simmons, D.J. Dwyer, Surf. Sci. **48**, 373 (1975)
12. C.F. Brucker, T.N. Rhodin, Surf. Sci. **57**, 523 (1976)
13. K.O. Legg, F. Jona, Phys. Rev. B **16**, 5271 (1977)
14. C.R. Brundle, Surf. Sci. **66**, 581 (1977)
15. Y. Sakisaka, T. Miyano, M. Onchi, Phys. Rev. B **30**, 6849 (1984)
16. R.L. Headrick, P. Konarski, S.M. Yalisove, W.R. Graham, Phys. Rev. B **39**, 5713 (1989)
17. S.J. Roosendaal, B. van Asselen, J.W. Elsenaar, A.M. Vredenberg, F.H.P.M. Habraken, Surf. Sci. **442**, 329 (1999)
18. V. Stambouli, C. Palacio, H.J. Mathieu, D. Landolt, Appl. Surf. Sci. **70-71**, 240 (1993)
19. F. Bisio, R. Moroni, M. Canepa, L. Mattera, Phys. Rev. Lett. **83**, 4868 (1999)